Bulk optical properties and tissue components in the female breast from multiwavelength time-resolved optical mammography

Lorenzo Spinelli
Alessandro Torricelli
Antonio Pifferi
Paola Taroni
INFM
Dipartimento di Fisica and IFN-CNR
Politecnico di Milano
Piazza Leonardo da Vinci 32
I-20133 Milan, Italy
E-mail: lorenzo.spinelli@fisi.polimi.it

Gian Maria Danesini
Casa di Cura S. Pio X
Dipartimento di Radiologia
via Francesco Nava 31
I-20159 Milan, Italy

Rinaldo Cubeddu
INFM
Dipartimento di Fisica and IFN-CNR
Politecnico di Milano
Piazza Leonardo da Vinci 32
I-20133 Milan, Italy

Abstract. We present the results of a clinical study about optical properties and bulk composition of the female breast. The clinical study involved more than 150 subjects that underwent optical mammography. A multiwavelength time-resolved mammograph designed to collect time-resolved transmittance images of the breast at different wavelengths in the range 637 to 980 nm is used to this purpose. From the absorption spectrum of the breast, the concentrations of the main tissue constituents, i.e., oxygenated and deoxygenated hemoglobin, lipid, and water, are obtained for a subset of 113 breasts. The lipid content of breast is estimated for the first time on such a large number of subjects. The total hemoglobin concentration, blood oxygen saturation, lipid, and water content of breast is correlated to demographic information collected during the trial. As expected, breast optical properties and components undergo huge variations among different subjects. Different constituents, however, show interesting correlation with clinical parameters such as age, breast size, body mass index, and mammographic parenchymal pattern. These results suggest that optical measurements on breasts can be exploited to obtain relevant information on breast tissue composition. © 2004 Society of Photo-Optical Instrumentation Engineers. [DOI: 10.1117/1.1803546]

1 Introduction

The use of red and near-infrared (NIR) light for studying the female breast as a possible alternative or complementary means to diagnose cancer and other pathologies, with respect to conventional techniques such as x-ray mammography and ultrasonography, has been the object of intense investigations in the last ten years. One of the advantages of using NIR light is the high sensitivity of such wavelength range to the concentration of the main absorbers constituting the breast, that is, hemoglobin in its oxygenated (O_2Hb) and deoxygenated (HHb) state, lipid, and water. Due to the ability to distinguish among these different constituents, optical techniques are useful to characterize the bulk composition of the breast tissue. If we also consider the high penetration depth and the total noninvasiveness of light at these wavelengths, one can understand the great interest in developing new instruments able to perform measurements on the breast.

Nowadays, a number of clinical studies have been performed or are in progress, exploiting either frequency-domain or time-resolved optical instruments, both in reflectance and in transmittance geometry.[1–11] The basic goals of these studies are the assessment of scattering and absorption properties of the female breast and their possible correlation to patho-physiological and demographic (e.g., age, body mass index) information. In terms of the total hemoglobin content (tHb $=$ HHb $+$ O_2Hb) and blood oxygen saturation (SO_2 $=$ O_2Hb/tHb), the results obtained are quite consistent, even if in most of the preliminary studies the contribution of water and lipid was neglected.[1,4,11] In a few cases, the relative content of water was kept constant, ranging from 20 to 40% of the overall volume composition, and the lipid contribution either was neglected or kept constant.[7,9] More recently, *in vivo* spectroscopic results[12–15] have shown that physiological processes and/or pathological causes may affect significantly the water and lipid content in the female breast. Therefore, for a complete characterization of the female breast, the contributions of lipid and water should not only be considered but also independently estimated. In this framework, we present the results about optical properties and bulk composition of breast, obtained from a systematic clinical trial still in progress, performed with a multiwavelength time-resolved optical mammograph and supported by the European project OPTIMAMM. Up to November 2003, the trial has involved more than 150 patients, with either benign (cyst) or malignant (cancer) lesions. In terms of volume, however, the lesion tissue accounts for less than 1% of the whole breast, so that the bulk properties reported here are essentially relative to healthy tissue. In this study, we focus our attention on the optical

Address all correspondence to Lorenzo Spinelli, Politecnico di Milano, INFM-Dipartimento di Fisica and IFN-CNR, Piazza Leonardo da Vinci 32, 1-20133 Milan, Italy. Tel: 39-02-23996097; Fax: 39-02-23996126; E-mail: lorenzo.spinelli@fisi.polimi.it

characteristics relative to 113 breasts belonging to a subset of the patients. Bulk HHb, O_2Hb, lipid, and water contents are derived, and correlation with demographic information is reported.

2 Materials and Methods

2.1 Optical Mammograph

The instrument is designed to collect time-resolved transmittance images, at different wavelengths, of the breast compressed between plane Plexiglas plates. During the clinical study, the instrument has undergone some upgrade by increasing the number of wavelengths adopted. Initially, four pulsed diode lasers (PDL Heads, PicoQuant, Germany) emitting at 683, 785, 913, and 975 nm, with average output power of ~1 to 4 mW, temporal width of ~180 to 400 ps [full width at half maximum (FWHM)], and repetition rate of 40 MHz were used as light sources. Then, up to seven light sources were adopted (637, 656, 683, 785, 912, 975, and 985 nm) with about the same power and temporal characteristics as before, while the repetition rate has been decreased to 20 MHz. A single driver (PDL-808 Sepia, PicoQuant, Germany) controls all the laser heads, and their output pulses are properly delayed by means of graded index optical fibers, and combined into a single coupler. A lens produces a 3-mm-diam collimated beam that illuminates the breast. A 5.6-mm-diam, 1-m-length fiber bundle collects the output light on the opposite side of the compression unit. The distal end of the bundle is bifurcated, and its two legs guide photons respectively to two photomultiplier tubes (PMTs) for the light detection (R5900U-01-L16 and H7422P-60, Hamamatsu, Japan). Variable neutral density circular filters, placed in front of each PMT, are used to optimize the illumination power for *in vivo* measurements and for the acquisition of the instrument response function, as changing the settings of the laser driver would affect the laser pulse duration and stability. A PC board for time-correlated single photon counting (SPC134, Becker and Hickl, Germany) allows the acquisition of time-resolved transmittance curves. The illumination fiber and collecting bundle are scanned in tandem with steps of 1 mm. A complete scan typically requires 5 min. The Plexiglas plates can be rotated, so that images of both breasts can be recorded in the cranio-caudal (CC) as well as oblique (OB-45 deg) views. Further technical details can be found in Ref. 16.

2.2 Measurement Protocol

In this study, optical images of both breasts have been routinely acquired in CC and OB views for each patient. The measurement protocol was approved by the local ethics committee, and informed consent was obtained from all women recruited for the clinical trial. Furthermore, demographic information relative to each patient was collected. Table 1 summarizes some pieces of information on the enrolled subjects.

2.3 Data Analysis

For each wavelength, images of the absorption and reduced scattering coefficients were obtained by fitting the time-resolved transmittance curves with a model based on the diffusion equation with extrapolated boundaries.[17] Two different fitting procedures were adopted. To investigate the behavior of breast optical properties, the time-resolved curves were fit-

Table 1 Mean, standard deviation (SD), and range of demographic parameters of the selected subjects.

Parameter	Mean	SD	Min	Max
Age (yr)	59.1	9.5	30	79
Breast thickness (cm)	4.5	1.1	2.2	7.0
BMI (kg m^{-2})	24.1	4.6	14.9	35.7

ted by assuming both absorption and reduced scattering coefficients as free fitting parameters. On the other hand, to characterize the breast in terms of tissue components, we fixed the value for the reduced scattering coefficient μ_S' and used μ_a and time shift as free fitting parameters. The latter fitting procedure, in fact, reduces the coupling between absorption and scattering coefficients, and consequently the dispersion in the fitted absorption coefficient μ_a.[18] To this purpose, at each wavelength the value of the reduced scattering coefficient was estimated as an average over several measurements performed with a broadband system for time-resolved reflectance spectroscopy.[19]

For each breast projection and wavelength, we selected a reference bulk area far from boundaries and eventual inhomogeneities. To automate the selection of the reference area, the distribution of time of flight (i.e., the first moment of the time-resolved transmittance curve) was calculated. Then, pixels were included in the reference area whenever the corresponding value of the time of flight was greater or equal to the median of the distribution. The absorption and reduced scattering spectra were then obtained by averaging the absorption and reduced scattering coefficients over the reference area.

Next, the absorption spectrum was interpreted as the linear combination of the extinction coefficients of HHb, O_2Hb, water,[20,21] and lipid,[22] weighted by their average concentration. This allowed us to obtain estimates for tHb, SO_2, lipid,
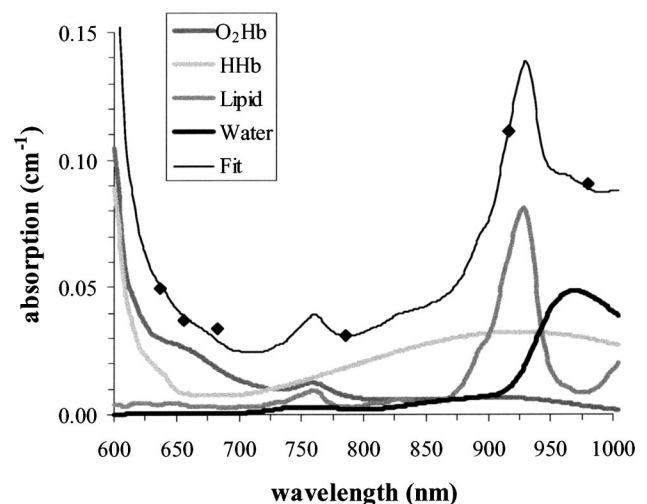

Fig. 1 Absorption spectrum of a breast (thin line), obtained as the sum of absorption spectra of the main breast constituents (thick lines). The measured values of the absorption coefficient (symbols) are also reported.
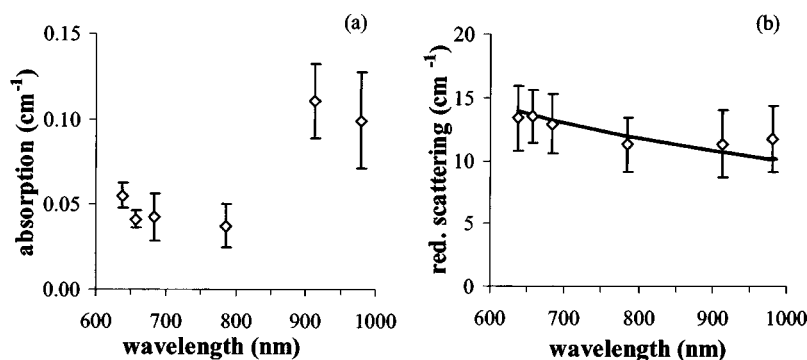
Fig. 2 Median values of (a) the absorption and (b) reduced scattering coefficients at different wavelengths. The error bars represent the dispersion of data over different subjects, breasts, and projections. The reduced scattering spectrum used in the fitting procedure is also reported (solid line).

and water content. The only assumption made in the derivation of these quantities was that the resulting estimate for each constituent had to be nonzero. To this purpose, we used an algorithm that solves linear systems by performing a least-squares procedure with non-negativity constraints on the unknowns (the lsqnonneg algorithm of Matlab—The MathWorks Incorporated[23]). An example of the absorption spectrum of the breast with spectra of the different constituents is reported in Fig. 1.

Finally, results are presented here for 113 breasts belonging to the subset characterized by normal physiological values of the tissue constituents, that is $tHb < 200 \, \mu M$, $SO_2 > 40\%$. We also excluded cases with the estimated total percentage of tissue constituents lower than 50% (ideal value should be 100%, but some constituents may not absorb in the red-NIR range.). Moreover, a preliminary filter was applied to include in the analysis only breasts with acceptable signal-to-noise ratio (SNR) at all measured wavelengths. In particular, we considered only breast images with at least 100 counts per pixel. This is the major cause of exclusion from further analyses, and is mostly due to the very low SNR at the longest wavelength, where water absorption dominates and detector sensitivity is low.

3 Results and Discussion

3.1 Optical Properties

Median values of the absorption and reduced scattering coefficients at the different wavelengths used in the clinical study

are reported in Fig. 2. These values were obtained by using both absorption and reduced scattering coefficient as free fitting parameters. Error bars represent the dispersion of data over different subjects, breasts (left and right), and projections (CC and OB). Table 2 shows the corresponding numerical values for an easier comparison with literature data. The reduced scattering spectrum used in the fitting procedure with fixed μ_S' is also depicted in Fig. 2(b).

Our results are consistent with data from Durduran et al.:[9] they found an average value of $0.041 \pm 0.025 \, cm^{-1}$ and $8.5 \pm 2.1 \, cm^{-1}$ at 780 nm for μ_a and μ_S', respectively. The lower value for the reduced scattering coefficient might be interpreted as a result of the different measurement geometry (patient lying versus sitting). Also, good agreement was found with the mean values reported by Grosenick et al.[7] They in fact report $0.041 \pm 0.013 \, cm^{-1}$ and $0.039 \pm 0.009 \, cm^{-1}$ for μ_a at 670 and 785 nm, respectively, while μ_S' is $11.7 \pm 2.3 \, cm^{-1}$ and $10.2 \pm 1.6 \, cm^{-1}$ at 785 nm. The scattering values are close to what we obtained, and also the measurement geometry is the same for both studies, in agreement with the previous hypothesis that the geometry might affect the estimated μ_S' values. Furthermore, we note that the dispersion of measured values is mostly due to the intersubject differences, with minor contributions from breast (left versus right) and projection (CC versus OB). These results have been confirmed also by broadband time-resolved reflectance and transmittance measurements performed with our laboratory system.[19] Therefore, the values reported in Table 2 could be considered as indicative of the female breast as a whole.

On the other hand, in a previous work on phantoms,[18] we have demonstrated that a fitting approach based on a fixed

Table 2 Median values and standard deviations for absorption and reduced scattering coefficients at different wavelengths.

Wavelength (nm)	Absorption (cm^{-1})	Reduced scattering (cm^{-1})
637	0.055 ± 0.007	13.4 ± 2.6
656	0.041 ± 0.005	13.5 ± 2.1
683	0.042 ± 0.013	12.9 ± 2.3
785	0.037 ± 0.013	11.3 ± 2.1
912	0.110 ± 0.021	11.4 ± 2.6
980	0.099 ± 0.028	11.7 ± 2.6

Table 3 Global mean, standard deviation (SD), and range of physiological parameters of breasts.

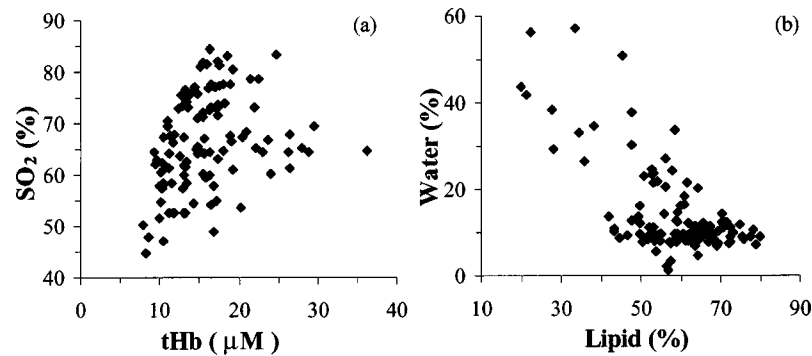| Property	Mean	SD	Min	Max
tHb (μM)	15.7	5.1	7.9	36.2
SO$_2$ (%)	66.4	9.2	44.7	84.4
Lipid (%)	58.0	12.1	20.0	79.7
Water (%)	14.5	10.7	1.2	57.2

Fig. 3 (a) Blood oxygen saturation as a function of the total hemoglobin content and (b) water content as a function of lipid content.

value for μ_S' and free values for μ_a and time shift improves linearity and lowers uncertainty as compared to a μ_a to μ_S' fit, especially for a low number of counts. Moreover, the dependence of results on the initial estimate of μ_S' is weak. Namely, a 20% error in the estimate of μ_S' [that is, about the mean difference between the actual μ_S' value and the fixed value used in the fitting procedure, as one can argue from Table 2 and Fig. 2(b)] yields less than 10% error on μ_a. As for the components, this means that, for example, an estimated lipid concentration of 50% is affected by an error of 5%. Furthermore, due to the linearity of this fitting procedure, the relative ratios between components are unchanged.

3.2 Tissue Components

We characterized each breast in terms of total hemoglobin concentration, blood oxygen saturation, lipid, and water content, taken as the average of the values obtained from the two projections. The global mean values, with standard deviation and range of the considered quantities, are reported in Table 3. Furthermore, we show the plot of SO_2 as a function of tHb [Fig. 3(a)] and water content as a function of lipid content [Fig. 3(b)] for each breast to visualize the distribution of these parameters among the subjects and to determine if some correlation exists among them. As for the latter, we note no correlation between blood oxygen saturation and blood content, while (as one would expect) at least in part of the subjects, water and lipid content are inversely related, even though most breasts are characterized by very low water content independent of the lipid content.

It is worth noting that the lipid concentration is estimated here for the first time in a large clinical study regarding bulk breast constituents. The mean values of different constituents reported in Table 3 are consistent with previously obtained values. In particular, lipid and water content agree with what Cerussi et al.[15] reported in their study. On the other hand, in a recent work, Srinivasan et al.[10] obtained quite higher values for water concentration (about 50% as a mean). We think that the mismatch between our values and theirs can be explained in two ways. First, as already mentioned, considering only data with high SNR, we probably sampled breasts with somehow lower water content than average. Second, in their study, Srinivasan et al. neglected the absorption of the lipid tissue. This fact could lead to an overestimation of the water content, because, even if the lipid extinction coefficient is lower in the spectral range considered (660 to 850 nm), the subjects participating in the study probably are characterized by a lipid content larger than water content.

To assess if these optically determined quantities are interesting for breast characterization, it is important to demonstrate that they correlate to the different parameters that are usually considered in clinics. For this reason, we have examined the lipid and water content, tHb and SO_2, as a function of the most important demographic information available from the clinical study, that is, body mass index (BMI); breast thickness (somehow related to breast volume), and age of the subjects. Furthermore, we have also analyzed the correlation with a clinical parameter that classifies the breast structure, such as the mammographic parenchymal pattern. This is a
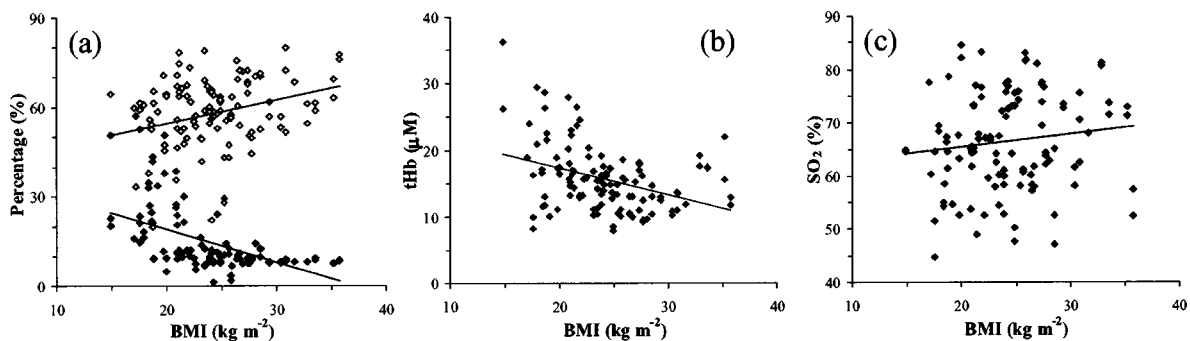

Fig. 4 (a) Lipid (open symbols) and water (closed symbols) concentrations, (b) total hemoglobin content, and (c) blood oxygen saturation as a function of body mass index.
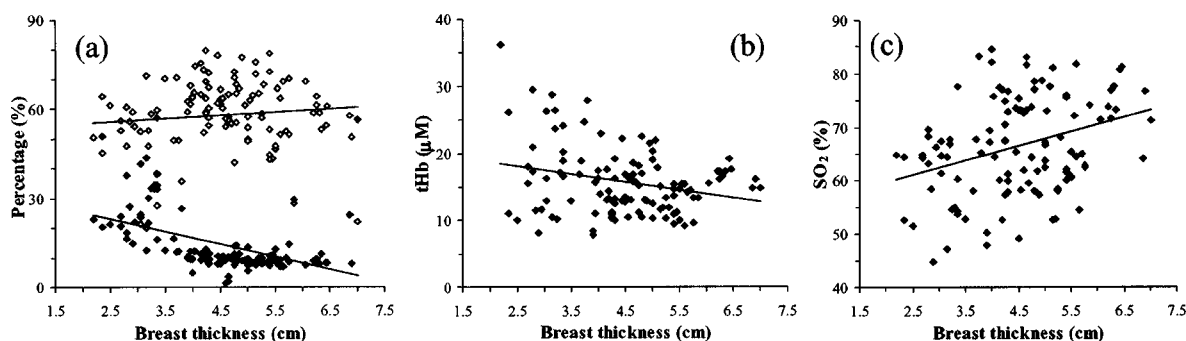
Fig. 5 (a) Lipid (open symbols) and water (closed symbols) concentrations, (b) total hemoglobin content, and (c) blood oxygen saturation as a function of breast thickness.

clinical parameter related to the radio-opacity of the breast and ruled by its structural composition. In particular, five mammographic parenchymal patterns can be identified according to Tabàr's classification.[24] Following this classification, pattern 1 refers to a breast with comparable content of adipose and fibrous tissues, while patterns 2 and 3 refer to breasts dominated by adipose tissue. On the other hand, patterns 4 and 5 classify breasts with prominent fibrous tissue, which increases their radio-opacity.

As for the correlation with BMI, Fig. 4 shows an increase in lipid content and a decrease in water content as the BMI increases. In terms of rate of change, we have a 0.78% of increase and a 1.1% of decrease per BMI unit for lipid and water content, respectively. This agrees with the fact that BMI represents a measure of the breast fat content. A further correlation was found with total hemoglobin content, which decreases with the BMI increase (-0.41 μM per BMI unit), in agreement with the fact that an increase of BMI means that the tissue has a lower vascular density. On the other hand, SO_2 is substantially independent of BMI.

By analyzing variations of different quantities as a function of the breast thickness (Fig. 5), we can note that for high thickness (above 4 cm), the water content stabilizes on a value of about 10%, which seems to be an indication of the minimal water content in the breast. Furthermore, we observe no significant trend in lipid and hemoglobin content and some increase in the blood oxygen saturation (2.7% of SO_2 per centimeter of breast thickness). This trend of SO_2 with respect to the increase of breast thickness is somehow unexpected, and we have not yet found a clear explanation for it.

In Fig. 6 we report the correlations of the optical parameters as a function of the subject age. The main trends are shown by the lipid and water components: as one would expect, the lipid content of breast increases with age, with adipose tissue progressively replacing the fibroglandular tissue that is richer in water content (as shown in Fig. 7 about the correlation of lipid and water content with the mammographic parenchymal pattern). The slopes of the trend lines give a 0.52% of lipid content increase per year of age and a 0.53% of water content decrease per year of age.

Then we considered the correlation of lipid and water content with the mammographic parenchymal pattern. We found a good correlation between the breast pattern and the lipid and water content. Figure 7 reports the mean values for lipid and water content as a function of the mammogaphic pattern. We can note how the content of lipid increases as we go from breasts of pattern 1 to breasts of pattern 3, while an increase in water content and a decrease in lipid content are observed when breasts of patterns 4 and 5 are considered.

4 Conclusions

We present results about the bulk composition of breast, in terms of total hemoglobin concentration, blood oxygen saturation, lipid, and water content, obtained from near-infrared spectroscopic measurements performed during a systematic clinical trial by means of a multiwavelength time-resolved optical mammograph. The data shown here refer to 113 breasts belonging to a subset of the patients involved in the clinical trial. As described before, only breasts with accept-
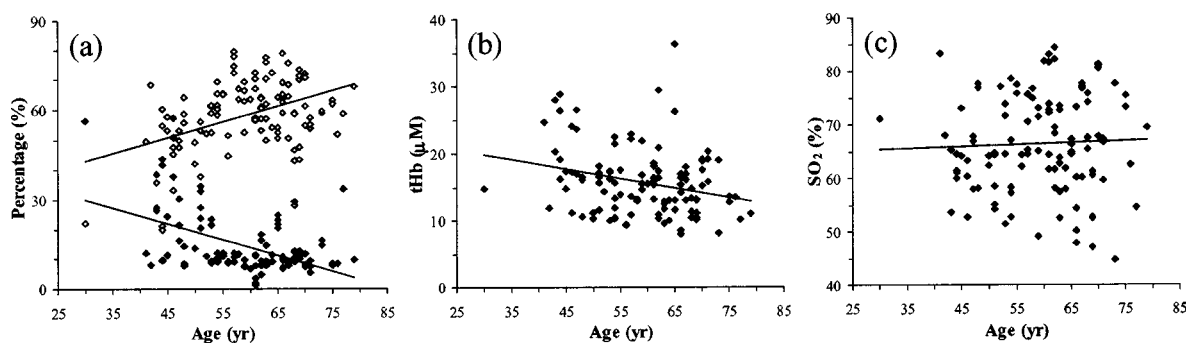

Fig. 6 (a) Lipid (open symbols) and water (closed symbols) concentrations, (b) total hemoglobin content, and (c) blood oxygen saturation as a function of subject age.
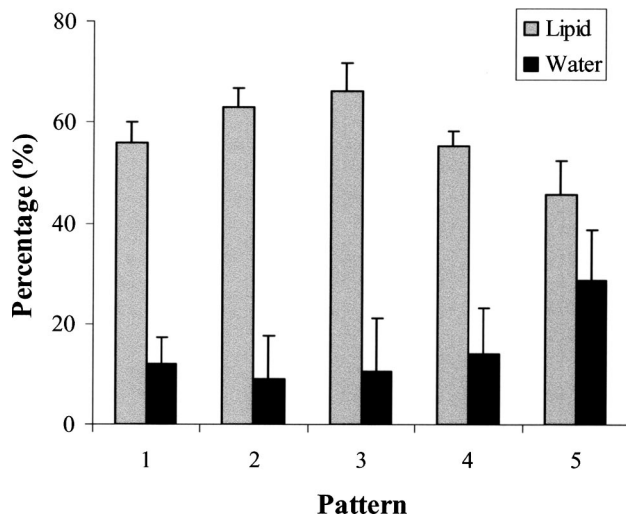
Fig. 7 Mean and standard deviation of lipid and water mean concentrations obtained for the different mammographic parenchymal patterns.

able SNR at all measured wavelengths are included in the analysis. The problem of very low SNR mainly affects the longest wavelengths, where water absorption dominates and detector sensitivity is lower. As a result, the presented data might represent a specific subset of the whole demographic range, likely characterized by low water content. Our results, as expected, correlate with demographic information, supporting the idea that optical measurements can be of interest in providing information about breast tissue composition. In this study, we focus on the absorbing properties of the breast. However, a more complete analysis regarding the capability of optical techniques for the characterization of the female breast must consider also the scattering properties of the breast and their correlations with the structural parameters. This will be the aim of future work. Nevertheless, we demonstrate that indications about breast structural characteristics in term of radio-opacity can be inferred also from the bulk composition, if the lipid content is fully considered.

References

1. H. Dehghani, B. W. Pogue, S. P. Poplack, and K. D. Paulsen, "Multiwavelength three-dimensional near-infrared tomography of the breast: initial simulation, phantom, and clinical results," *Appl. Opt.* **42**, 135–145 (2003).
2. H. Jiang, Y. Xu, N. Iftimia, J. Eggert, K. Klove, L. Baron, and L. Fajardo, "Three-dimensional optical tomographic imaging of breast in a human subject," *IEEE Trans. Med. Imaging* **20**, 1334–1340 (2001).
3. V. Ntziachristos, A. G. Yodh, M. Schnall, and B. Chance, "Concurrent MRI and diffuse optical tomography of breast after indocyanine green enhancement," *Proc. Natl. Acad. Sci. U.S.A.* **97**, 2767–2772 (2000).
4. S. B. Colak, M. B. van der Mark, G. W.'t Hooft, J. H. Hoogenraad, E. S. van der Linden, and F. A. Kuijpers, "Clinical optical tomography and NIR spectroscopy for breast cancer detection," *IEEE J. Sel. Top. Quantum Electron.* **5**, 1143–1158 (1999).
5. K. T. Moesta, S. Fantini, H. Jess, S. Totkas, M. A. Franceschini, M. Kaschke, and P. M. Schlag, "Contrast features of breast cancer in frequency-domain laser scanning mammography," *J. Biomed. Opt.* **3**, 129–136 (1998).
6. L. Götz, S. H. Heywang-Köbrunner, O. Schötz, and H. Siebold, "Optical mammography on preoperative patients (Optische Mammographie an pra operativen Patientinnen)," *Aktuelle Radiol.* **8**, 31–33 (1998).
7. D. Grosenick, K. T. Moesta, H. Wabnitz, J. Mucke, C. Stroszczynski, R. Macdonald, P. M. Schlag, and H. Rinneberg, "Time-domain optical mammography: initial clinical results on detection and characterization of breast tumors," *Appl. Opt.* **42**, 3170–3186 (2003).
8. P. Taroni, G. Danesini, A. Torricelli, A. Pifferi, L. Spinelli, and R. Cubeddu, "Clinical trial of time-resolved scanning optical mammography at 4 wavelengths between 683 and 975 nm," *J. Biomed. Opt.* **9**(3), 464–473 (2004).
9. T. Durduran, R. Choe, J. P. Pulver, L. Zubkov, M. J. Holboke, J. Giammarco, B. Chance, and A. G. Yodh, "Bulk optical properties of healthy female breast tissue," *Phys. Med. Biol.* **47**, 2847–2861 (2002).
10. S. Srinivasan, B. W. Pogue, S. Jiang, H. Dehghani, C. Kogel, S. Soho, J. J. Gibson, T. D. Tosteson, S. P. Poplack, and K. D. Paulsen, "Interpreting hemoglobin and water concentration, oxygen saturation, and scattering measured *in vivo* by near-infrared breast tomography," *Proc. Natl. Acad. Sci. U.S.A.* **100**, 12349–12354 (2003).
11. X. Cheng, J. Mao, R. Bush, D. B. Kopans, R. H. Moore, and M. Chorlton, "Breast cancer detection by mapping hemoglobin concentration and oxygen saturation," *Appl. Opt.* **42**, 6412–6421 (2003).
12. R. Cubeddu, A. Pifferi, P. Taroni, A. Torricelli, and G. Valentini, "Non-invasive absorption and scattering spectroscopy of bulk diffusive media: An application to the optical characterization of human breast," *Appl. Phys. Lett.* **74**, 874–876 (1999).
13. B. J. Tromberg, N. Shah, R. Lanning, A. Cerussi, J. Espinosa, T. Pham, L. Svaasand, and J. Butler, "Non-invasive in vivo characterization of breast tumors using photon migration spectroscopy," *Neoplasia* **2**, 26–40 (2000).
14. R. Cubeddu, C. D'Andrea, A. Pifferi, P. Taroni, A. Torricelli, and G. Valentini, "Effects of the menstrual cycle on the visible and near infrared optical properties of the human breast," *Photochem. Photobiol.* **72**, 383–391 (2000).
15. A. E. Cerussi, D. Jakubowski, N. Shah, F. Bevilacqua, R. Lanning, A. J. Berger, D. Hsiang, J. Butler, R. F. Holecombe, and B. J. Tromberg, "Spectroscopy enhances the information content of optical mammography," *J. Biomed. Opt.* **7**, 60–71 (2002).
16. A. Pifferi, P. Taroni, A. Torricelli, F. Messina, R. Cubeddu, and G. Danesini, "Four-wavelength time-resolved optical mammography in the 680 to 980 nm range," *Opt. Lett.* **28**, 1138–1140 (2003).
17. D. Contini, F. Martelli, and G. Zaccanti, "Photon migration through a turbid slab described by a model based on diffusion approximation. I. Theory," *Appl. Opt.* **36**, 4587–4599 (1997).
18. R. Cubeddu, A. Pifferi, P. Taroni, A. Torricelli, and G. Valentini, "Experimental test of theoretical models for time-resolved reflectance," *Med. Phys.* **23**, 1625–1633 (1996).
19. A. Pifferi, J. Swartling, E. Giambattistelli, E. Chikoidze, A. Torricelli, P. Taroni, M. Andersson, A. Nilsson, and S. Andersson-Engels, "Multidistance optical characterization of the female breast by time-resolved diffuse spectroscopy," *Proc. SPIE* **5138**, 6–11 (2003).
20. S. Prahl, Oregon Medical Laser Center website, see http://omlc.ogi.edu/spectra/water/index.html.
21. S. J. Matcher, C. E. Elwell, C. E. Cooper, M. Cope, and D. T. Delpy, "Performance comparison of several published tissue near-infrared spectroscopy algorithms," *Anal. Biochem.* **227**, 54–68, (1995).
22. R. L. P. van Veen, A. Pifferi, A. Torricelli, E. Chikoidze R. Cubeddu, and H. J. C. M. Sterenborg, "Determination of VIS-NIR absorption coefficients of mammalian fat, with time- and spatially resolved diffuse reflectance and transmission spectroscopy" (submitted for publication).
23. C. L. Lawson and R. J. Hanson, *Solving Least Squares Problems*, Prentice-Hall, Englewood Cliffs, NJ (1974).
24. T. Gram, E. Funkhouser, and L. Tabàr, "The Tabàr classification of mammographic parenchymal patterns," *Eur. J. Radiol.* **24**, 131–136 (1997).